MASS TRANSFER BETWEEN BUBBLES AND SEAWATER

Jan Erik OLSEN, Dorien DUNNEBIER, Emlyn DAVIES, Paal SKJETNE and John MORUD

SINTEF Materials & Chemistry

ABSTRACT

Mass transfer between bubbles and seawater is an important mechanism when determining how much gas reaches the atmosphere from gas sources at the seabed. The mass transfer coefficient is a governing parameter for the phenomenon. Experiments on small bubbles in seawater have been performed where the bubble size has been monitored. The observed evolution of the bubble size has been compared with theoretical predictions of the bubble size. Based on this comparison, it is shown that mass transfer correlations for contaminated conditions is more consistent with experiments than correlations for clean conditions. It is also learned that simultaneous desorption of gases dissolved in the liquid must be accounted for.

NOMENCLATURE

A	surface area, m^2	Re	Reynolds number
C	coefficient	Sc	Schmidt number
c	concentration, kg/m^3	μ	viscosity, Pa s
D	diffusivity, m^2/s	ρ	density, kg/m^3
Eo	Eotvos number	σ	surface tension, Nm
d	diameter, m		
g	constant of gravity, m^2/s	Indexes	
H	Henri's constant, kg/m^3Pa	b	bubble
J	flux, kg/m^2s	D	drag
k	mass transfer coefficient, m/s	i	species
$\dot{m}_i$	mass transfer rate, kg/s	l	liquid
P	pressure, Pa	t	terminal

1 INTRODUCTION

Mass transfer between bubbles and seawater is an important mechanism in subsea blowouts and seepage from natural sources at the seabed. Being able to quantify mass transfer enables assessment of how much gas is dissolved in the ocean and how much gas reaches the atmosphere. Accumulation of methane in the atmosphere contributes to global warming. Although there are uncertainties in the significance of the marine contribution to atmospheric methane, studies exist which support the importance of natural gas seeps at the seabed [1]. During accidental subsea blowouts from gas wells or pipelines, the amount and composition of gas reaching the atmosphere determines the potential for fire and explosions [2].

Mass transfer between gas bubbles and surrounding liquid depends on solubility and the ability of the liquid to transport the gas species away from the bubble surface by convection and diffusion [3]. The contribution from convection and diffusion can be assigned to a mass transfer coefficient. The mass

transfer rate is proportional this coefficient, which thus is essential in determining the fate of rising bubbles [3, 4]. It is affected by several parameters including bubble size, diffusivity and level of contamination in the liquid. This requires thorough investigations of conditions where these correlations are valid before they can be applied. Numerous correlations exist for the mass transfer coefficient (e.g. [5-10]).

In the study presented here, an objective has been to assess if some of the previously published correlations are consistent with experimental data on bubbles in seawater. Although many experiments on mass transfer from bubbles have been conducted, very few of these have been performed with seawater. Some of the experiments with fresh water are still relevant for the topic. Takemura and Yabe [11] conducted experiments on rising CO_2 bubbles in degassed water, both clean and contaminated. They designed a camera system where the camera moved alongside the rising bubbles. Alves *et.al.* [12] performed experiments in a downward flowing water column where they could maintain a fixed position of air bubbles for observations with various levels of contamination. More recently [13] measured bubble size evolution on CO2 bubbles in a vertical pipe with controlled levels of surfactants. All of these investigations conclude that mass transfer varies with contamination and that mass transfer decreases with increasing contamination. Mass transfer of bubbles in seawater was studied by Rehder *et.al.* [14] by measuring the evolution of bubble size on large bubbles (2-8 mm) released at deep waters (>400 m) outside Monterey. In order to match these experimental results Leifer and Patro [3] and McGinnis *et.al.* [4] needed to apply correlations for mass transfer coefficients for clean or partly contaminated conditions. Correlations for fully contaminated conditions were inconsistent with the experiment. Concentration of surfactants were not measured.

The study presented here focusses on smaller bubbles (<1 mm) in shallow seawaters (< 80 m). Experiments were conducted in a counter-current system, similar to the experiments of Alves *et.al.* [12], fed by a continuous supply of seawater. Temporal evolution of bubble size was monitored over durations of up to 20 minutes. The theory for mass transfer on bubbles is then compared with the experimental results and various correlations for the mass transfer coefficients results are assessed. Theory, experimental setup and results from the study are described with the goal of acquiring more information regarding the mass transfer between bubbles and seawater.

2 THEORY

A challenge in modelling gas-liquid mass transfer for bubbles is to choose a proper mass transfer coefficient. The mass transfer coefficient quantifies how fast species are moving across an interphase. The mass transfer coefficient typically depends on how fast the species diffuse or are convected to and from the interphase. Typically for a gas bubble in a liquid, the limiting transport rate is located on the liquid side of the interphase. Therefore, species diffusion in the liquid and convective transport to and from the boundary layer on the liquid side will determine the mass transfer coefficient. The relevant convective velocity scale for transport to and from the liquid interface is the so called slip velocity between the bubble and the bulk liquid. Mass transfer also depends on whether surfactants and other contaminants are present at the interphase. Thus, correlations for the mass transfer coefficient exist for both clean and contaminated systems. A clean system is typically distilled water. Since seawater is naturally occuring and not treated in any way, it intuitively feels like it is a contaminated system. Note that an intermediate condition known as partly contaminated is normally also introduced (see below). The theory below describes mass transfer of a species to or from a gas bubble with a surrounding liquid in clean and contaminated systems.

The concentration of dissolved gaseous species in the ocean are normally very small and thus the principles of Fickian diffusion is assumed. Since diffusion and mass transfer is much faster in gas than

in liquids, we can assume that all mass transfer resistance exist on the liquid side of the gas-liquid interphase. Mass transfer of species *i* from a bubble to the surrounding liquid is then given by [15]

$$\dot{m}_i = A_b J_i = \pi d_b^2 \cdot k_i^l \cdot (c_i^{sol} - c_i^l) \quad (1)$$

Here d_b is the bubble diameter (representing surface area), k_i^l is the mass transfer coefficient for species *i* in the surrounding liquid, c_i^{sol} is the solubility of species *i* in the surrounding liquid and c_i^l is the concentration of species *i* in the surrounding liquid. The solubility c_i^{sol} depends on partial pressure, temperature and salinity. For an ideal gas mixture we can apply Henry's law and use [3]

$$\dot{m}_i = A_b J_i = \pi d_b^2 \cdot k_i^l \cdot \left(H_i P_i - c_i^l\right) \quad (2)$$

where P_i is the partial pressure of species *i*, H_i is Henry's constant[1] for solubility of species *i*. Use of this should be limited to moderate pressures. In the comparison between experiments and theory below Eq.2 is applied, but for deep sea conditions Eq.1 should be applied.

The mass transfer coefficient is a governing parameter when estimating the mass transfer rate. The coefficient strongly depends on whether contaminants are present or not. This is seen in Figure 1. Based on penetration theory, Higbie [8] derived a correlation for mobile interphases (clean conditions). This is considered as a theoretical upper limit on the mass transfer coefficient. Contaminated water usually has surface active components known as surfactants. In seawater this is mainly polysaccharides [16]. Surfactants will immobilize the interphase. Frössling derived an expression for rigid interphases (contaminated conditions) from laminar boundary layer theory that acts as a lower limit. Several other correlations also exist, either based on more advanced theory or experimental observations, e.g. [5, 9]. If contaminants are present in relatively small concentrations such that fast rising bubbles (typically large bubbles) are able to shed the surrounding layer of contaminants, the term partly contaminated is used. In partly contaminated conditions, small bubbles will behave as contaminated and large bubbles as clean. The transition can be explained by a stagnant cap model [17] which was supported by the experiments of Takemura and Yabe [11] and Alves *et.al.* [12]. Based on these findings, correlations for partly contaminated systems have been derived, e.g. [6]. Normally only distilled water qualifies as clean conditions. Thus partly contaminated or contaminated is expected to be the condition experienced by the bubbles in seawater. Even if we narrow the condition down to one of these two, there are still several proposed correlations for the mass transfer coefficient. The above mentioned correlations are listed in Table 1. These correlations depend on slip velocity of bubbles u_b, bubble diameter d_b, diffusivity of species *D*, Reynolds number

$$Re = \frac{\rho_l d_b u_l}{\mu_l} \quad (3)$$

[1] Note that numerous definitions of Henry's constants exist since both pressure and concentration can be specified in various units.

and Schmidt number

$$Sc = \frac{\mu_l}{\rho_l D} \qquad 4$$

Table 1: Correlations for mass transfer coefficients (m/s).

Higbie[8]	Clean	$\frac{2}{\sqrt{\pi}}\sqrt{Re\ Sc}\ \frac{D}{d_b}$
Clift et.al.[6]	Partly contaminated	$\frac{2}{\sqrt{\pi}}\sqrt{1-\frac{2.89}{\max(2.89,\sqrt{\mathrm{Re}})}}\ \mathrm{Re}^{1/2}\mathrm{Sc}^{1/2}\ \frac{D}{d}$
Bird[5]	Contaminated	$\sqrt{4+1.21\cdot \mathrm{Re}^{2/3}\mathrm{Sc}^{2/3}}\ \frac{D}{d_b}$
Hughmark[9]	Contaminated	$\left(2+0.95\cdot \mathrm{Re}^{1/2}\mathrm{Sc}^{1/3}\right)\frac{D}{d_b}$
Frössling[7]	Contaminated	$0.6\sqrt{u_b/d_b}\ D^{2/3}\left(\mu/\rho\right)^{-1/6}$

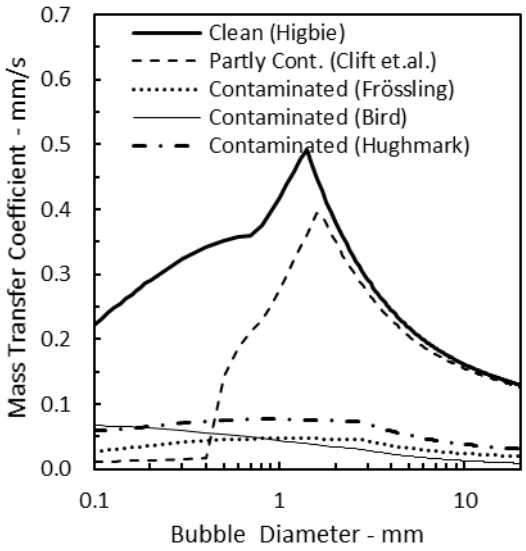

Figure 1: Correlations for mass transfer coefficient for clean, partly contaminated and contaminated bubbles.

The mass transfer coefficient is quite sensitive to the slip velocity of the bubbles. The slip velocity is the relative velocity between the bubble and the background liquid. It is governed by a force balance including gravity (buoyancy) and viscous drag. When gravity and drag are in equilibrium, the bubble achieves a constant velocity known as the terminal velocity:

$$u_t = \sqrt{\frac{4}{3}\frac{g d_b}{C_D}\frac{\rho_l - \rho_b}{\rho_l}} \qquad 5$$

The terminal velocity has been used as slip velocity in the correlation above when extracting numbers for the plots in Figure 1. The drag coefficient C_D in Eq.5 is that of Tomiyama et.al. [18] as shown in Table 2. Here Eo is the Eotvos number

$$\mathrm{Eo} = \frac{(\rho_l - \rho_b) g d_b^2}{\sigma} \qquad 6$$

which quantifies the importance of buoyancy relative to surface tension. These correlations and Eq.5 give drag coefficient and terminal velocity as function of bubble size as illustrated in Figure 2 and Figure 3. The curves in Figures 1-3 are obtained by iterating the correlations in Table 1 and 2 and Eq.(5). The non-monotonous behaviour is caused by the non-monotonous expression for the drag coefficient in Table 2. The sharp transition marks a transition from spherical to non-spherical bubbles.

Table 2: Drag coefficient for clean, partly contaminated and contaminated conditions.

Clean	$C_D = \max\left\{\min\left[\frac{16}{\mathrm{Re}}(1+0.15\mathrm{Re}^{0.687}), \frac{48}{\mathrm{Re}}\right], \frac{8}{3}\frac{\mathrm{Eo}}{\mathrm{Eo}+4}\right\}$
Partly contaminated	$C_D = \max\left\{\min\left[\frac{24}{\mathrm{Re}}(1+0.15\mathrm{Re}^{0.687}), \frac{72}{\mathrm{Re}}\right], \frac{8}{3}\frac{\mathrm{Eo}}{\mathrm{Eo}+4}\right\}$
Contaminated	$C_D = \max\left\{\frac{24}{\mathrm{Re}}(1+0.15\mathrm{Re}^{0.687}), \frac{8}{3}\frac{\mathrm{Eo}}{\mathrm{Eo}+4}\right\}$

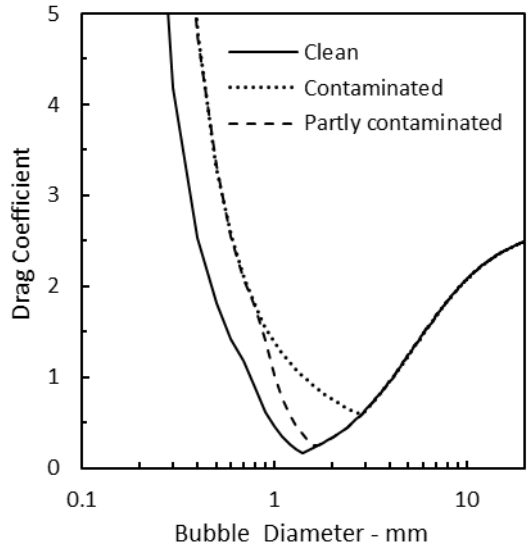

Figure 2: Drag coefficient as function of bubble diameter for clean, partly contaminated and contaminated conditions

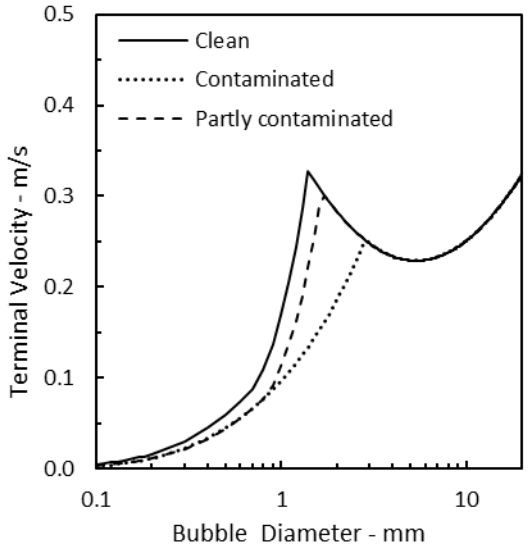

Figure 3: Terminal velocity as function of bubble diameter for clean, partly contaminated and contaminated conditions

3 EXPERIMENTAL WORK

A series of experiments were performed using a laboratory counter-current system for releasing rising gas bubbles into a carefully controlled downward flow of seawater. The objective of the design of the laboratory system is to create flow conditions such that a bubble will position itself at fixed location for observations by a stationary imaging system. The concept of employing a controlled vertical counter-current to stabilize buoyant bubbles, droplets, or particles was first proposed by Maini and Bishnoi [19] to investigate hydrate formation on natural gas bubbles, and subsequently employed by other researchers (e.g Alves *et.al.* [12], Nagamine [20];Masutani and Adams [21]).

The experimental system (Figure 4) is fed by a continuous source of filtered seawater, removing the need for a recirculating flow-through system (the out-flowing seawater is disposed of). This means that the system is 'pump-free', with the downward current being gravity fed, and controlled by a needle valve (flow controller) that changes the constriction of the outlet at the bottom of the system. The seawater is fed into the system through a seawater inlet at a depth of 80 meters in Trondheimsfjord, and filtered to remove particulate material above 4 microns.

The experimental approach is initialised by injection of buoyant gas bubbles (CH_4, CO_2 or N_2), which are released within a small turbulent jet and rise through an inverted Imhoff cone that creates a gradually increasing downward velocity (Figure 4). The Imhoff cone is positioned 2 meters above the release source and remnants of the turbulence in the release flow are dissipated before reaching the observation zone in the Imhoff cone. There is a group of bubbles released simultaneously, but to due to difference in size only one will be captured in the imaging zone. The larger ones will move through and smaller ones will position themselves further down in the Imhoff cone due the velocity gradient. At a given point, the drag forces on the bubble, due to the downward flow of water around it, balance the buoyancy force and the bubble become *captured*. Adjustments in the water speed are then made to relocate the bubble so it is suspended in the constant-area / imaging section where it is observed and quantified over time. These adjustments to flow are made to capture gas bubbles. This is achieved via adjustment of a needle valve controlling the drainage rate of seawater from the system. A constant resupply of seawater to the top of holding tank ensures a constant hydrostatic pressure, and thus, a highly controllable and stable downward velocity. An automated particle tracking and imaging system that is integral to the facility is used for quantification of changes to bubble size and shape over time. By this means, buoyant bubbles rising through the oceanic water column can be simulated (disregarding pressure effects). The diameter of the imaging zone is 25 mm. Compared to bubble diameters of roughly 0.2-2 mm, this diameter assures that there are no wall effects and no tendency to form Taylor bubbles. The top part of the imaging zone is also designed to minimize boundary layer effects on the flow and thus reducing turbulence. With the given configuration and the experienced terminal velocity of the bubbles the bubble Reynolds number is typically 20-200 and the hydraulic Reynolds number typically 1000-4000 ensuring that laminar flow dominates the mass transfer according to the criteria of Rzehak [22].

The general approach for using the counter-current system for studying the fate of gas bubbles is to establish a downward current that is in approximate equilibrium with the terminal rise velocity of the bubbles and quantify their behaviour over time (e.g. reduction in volume over time). Each bubble-capture experiment consists of the following steps:

1) Bubbles are released into downward-flowing seawater
2) The current velocity created by the flow control system keeps the bubble stable/focused in one position in the imaging section.

3) Current velocities are tuned to raise the bubbles into the imaging section for long-term monitoring.
4) The fate of a captured bubble is monitored and documented with the fixed imaging system.

Gases both in the bubbles and dissolved in the surrounding seawater move through the surface of the bubble [3]. As such, measurement of the decreasing bubble size over time will not yield a dissolution rate for a particular gas, as there is also an influx of other gases into the bubble from the surrounding seawater.

Artificial natural gas (later referred to as methane) was utilized to create one class of gas bubbles. The artificial natural gas was composed of the following gasses (presented as a percentage of the whole by mass): methane (92.8%), ethane (3.8%), propane (0.4%), carbon dioxide (0.6%), and nitrogen (2.4%). For this bubble class it was possible to measure its methane concentration. This was carried out in addition to the above four experimental steps. After a particular gas bubble was released from the imaging section, it was captured just prior to surfacing and was injected into a gas chromatograph (GC) to measure concentrations of methane. The GC used to measure the concentrations of methane had a flame ionization detector (FID) and a capillary designed to separate the C1-C5 gases.

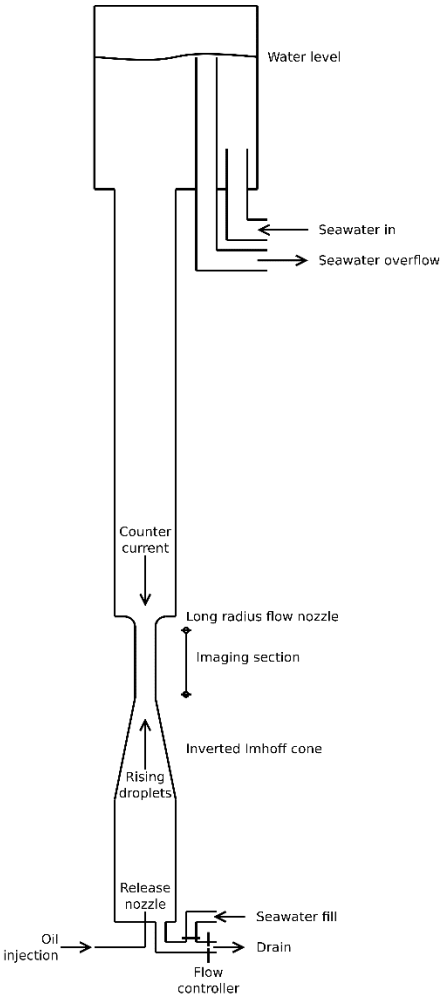

Figure 4: Schematic drawing of the laboratory counter-current system.

Due to the cylindrical geometry of the counter-current system, the use of classical particle sizing methods such as laser diffraction (e.g. LISST-100 / Malvern Mastersizer) is challenging. As such, bubble

size is measured using a silhouette-based, telecentric imaging system outlined in Figure 5. The distortion created by the curvature of the walls of the counter-current chamber is mostly removed by a square, water-filled outer box that created flat faces through which images are obtained. The distortion from refraction through the inner wall is therefore minimized. The imaging system has been calibrated against a dual-axis stage micrometer, which provided pixel sizes that were very close to the theoretical pixel size for the camera and lens configuration. A conservative minimum resolvable bubble diameter (d_b^{min}) of 80μm is used, based on the following relationship to pixel size:

$$d_b^{min} = \left\lceil 2\sqrt{\frac{24P_s^2}{\pi}} \right\rceil \qquad 7$$

where P_s is pixel size, which is 14.3μm for the camera and lens configuration used in these tests. This ensures that the smallest recorded bubble size contains 24 pixels in area.

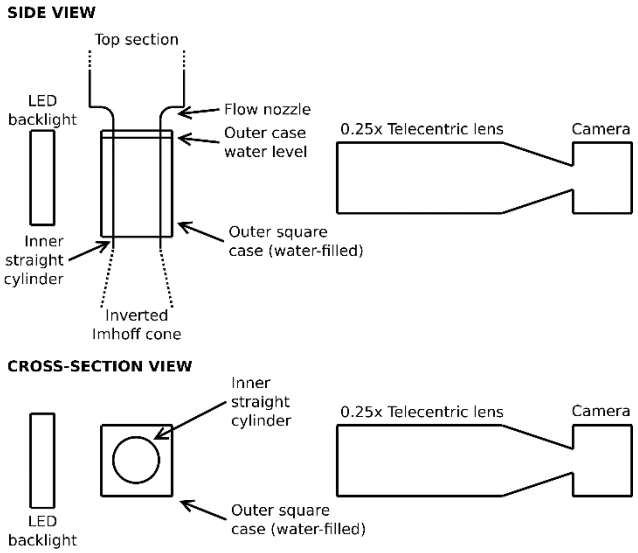

Figure 5: Schematic overview of the configuration of the imaging system and square case used to reduce distortion.

4 RESULTS AND DISCUSSION

Experiments were performed with 3 gases: N_2, CO_2 and CH_4[2] with seawater piped from 80 meters of approximately 10°C and 33 PSU (salinity) with observations taken at a depth of 2 meters. The bubble size was recorded by the aforementioned imaging system and terminal velocity was calculated from the calibrated flow control unit. Several repeated experiments were done for each gas. Based on quality of data acquisition, 5 sets of data for each gas was collected for comparison with the theory mentioned above.

The equations listed in Section 2 enable a model which predicts the terminal velocity of the bubble, the mass transfer rate and bubble diameter as function of time. The model requires an initial bubble diameter and material properties such as diffusivity, solubility, viscosity and density. Solubility varies with pressure, temperature and salinity [23-26]. Diffusivity depends on temperature and salinity, and

[2] The CH_4 bubbles were actually natural gas with 92.8% CH_4. For practical purposes we assume this as pure CH_4 bubbles. Table 3 shows that the properties of the other species are at the same order of magnitude as methane.

correlates with viscosity [27, 28]. These are listed in Table 3 for the water conditions mentioned above and a pressure corresponding to a 2 meter water depth. CO_2 is by far the most soluble gas. Ideal gas is assumed for density of gas. The properties of seawater varies with temperature and salinity. Alves *et.al.* [12]The properties [29] are listed in Table 4 for the given conditions.

Table 3: Solubility and diffusivity of chemical species involved in experiment

	Solubility mmol/mol	Diffusivity mm^2/s
CO2	0.9556	0.00128
CH4	0.0318	0.00074
N2	0.0108	0.00134
O2	0.0059	0.00161
C2H6	0.0466	0.000598
C3H8	0.0389	0.000476

Table 4: Properties of seawater at 10°C, 2 bar and 33 PSU

Density	1027	kg/m^3
Viscosity	1.4	mPa s
Surface tension	0.076	Nm

The diameter of the methane bubbles obtained experimentally and predicted with the model for different choices of mass transfer coefficient is seen in Figure 6. The left hand side of Figure 6 represents a chosen experiment while right part represents five experiments where bubble diameter is normalized with respect to bubble diameter as observed initially in each of these experiments. The normalization allows for visualization of multiple experiment in one figure. The bubble diameter decreases due to net outflux of gas species to the surrounding seawater. The bubbles which started out as methane bubbles loses the methane content faster than the observed and predicted evolution of the bubble diameter. The mismatch is caused by an influx of nitrogen and oxygen that is present in seawater. This is illustrated in Figure 7. We see that the bubble is almost depleted of methane in 3 minutes (a 0.5 mm bubble) whereas the bubble itself survives for more than 20 minutes. The GC measurements of methane concentration was carried out for a limited set of experiments and only one bubble was captured before it was depleted of methane. Although limited, the experimental results confirm that the bubbles lose methane on the same time scale as seen in Figure 7. Other gas components were not recorded, but the most plausible explanation is that the bubble absorbs nitrogen and oxygen as predicted by the theory. A single component gas model would not be able to predict this.

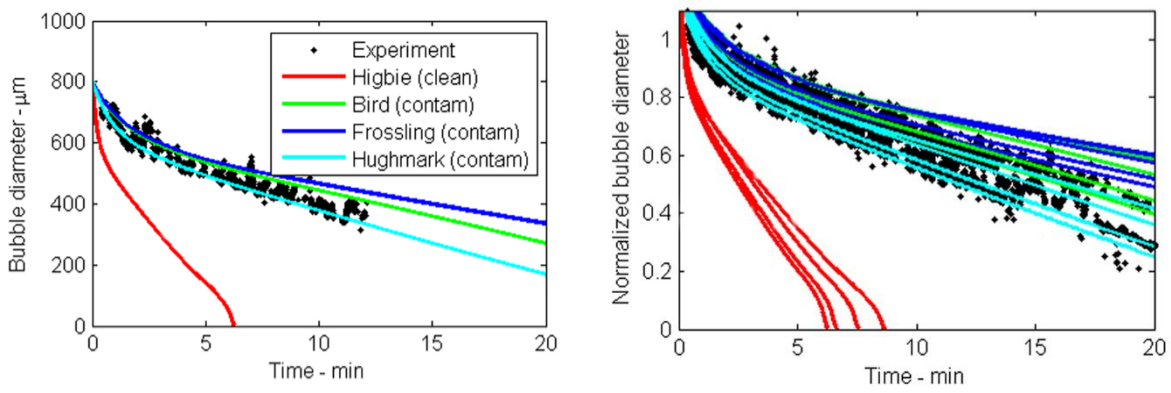

Figure 6: Bubble diameter as function of time for methane bubbles. Left part represents a chosen experiment while right part represents five experiments where bubble diameter is normalized with initial bubble diameter.

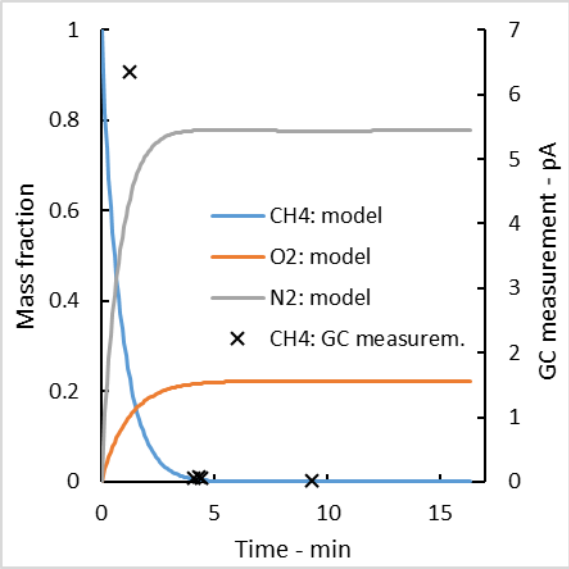

Figure 7: Mass fraction of bubble species GC readings of methane concentration as function of time for an initial methane bubble.

The results seen in Figure 6 show that correlations for mass transfer coefficient based on the assumption of clean conditions are inconsistent with experimental results. Correlations for contaminated conditions are quite consistent with the experiments. In particular, the correlation of Hughmark gives a good match between theory and observations. The same comparison between model and experiments were done for CO_2 and N_2. The comparison is shown in Figure 8 and Figure 9 for CO_2 and N_2 respectively. Due to the high solubility of CO_2, the bubbles are depleted of CO_2 within seconds. This is not resolved by the experiments since some time was required to capture the bubbles for observation. However this is confirmed by the experiments of Takemura and Yabe [11]. They measured bubble shrinkage of CO_2 bubbles in degassed water and observed that CO_2 bubbles completely dissolved within 5 seconds in contaminated water. For both CO_2 and N_2 the same trend is seen as for CH_4 when comparing theory and observations – correlations for clean conditions are inconsistent with observations and correlations for contaminated systems are consistent with observations. The correlation for mass transfer coefficient of Hughmark reproduces the experimental results very well.

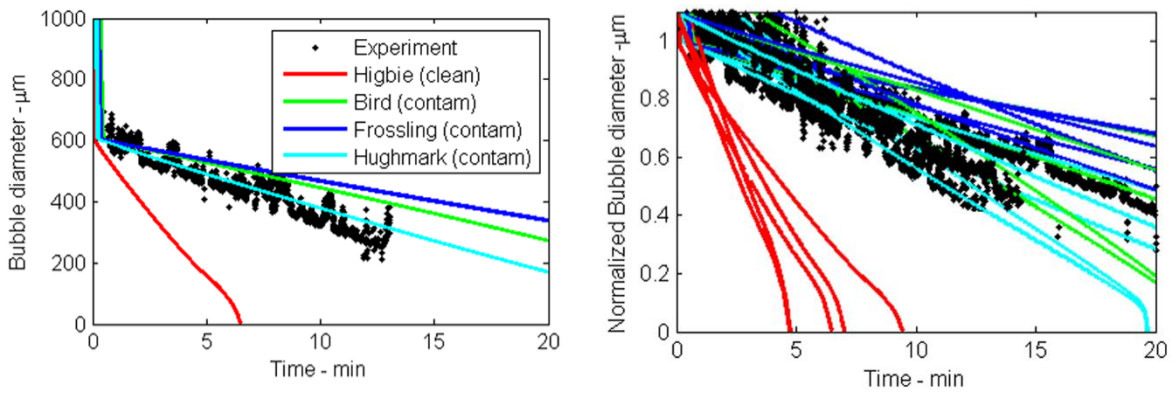

Figure 8: Bubble diameter as function of time for CO_2 bubbles. Left part represents a chosen experiment while right part represents five experiments where bubble diameter is normalized with initial bubble diameter.

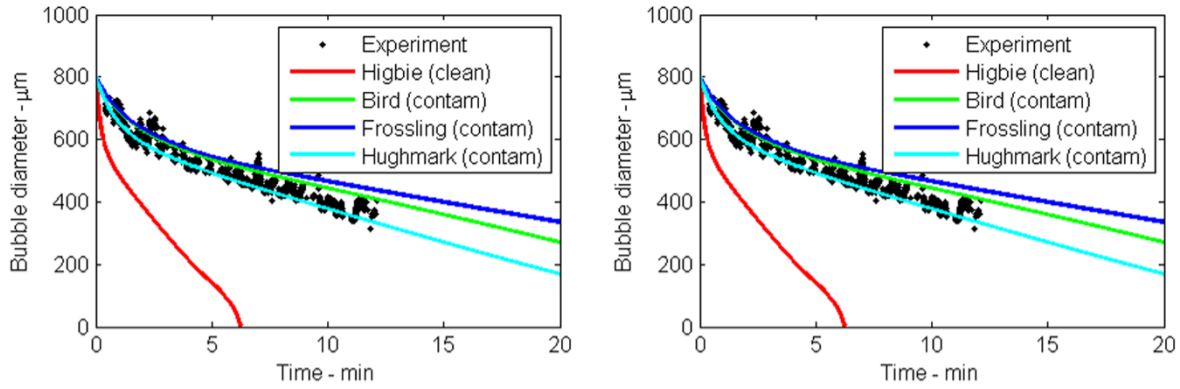

Figure 9: Bubble diameter as function of time for N_2 bubbles. Left part represents a chosen experiment while right part represents five experiments where bubble diameter is normalized with initial bubble diameter.

Since seawater is not distilled or treated in any way to remove surfactants, it is expected that that mass transfer in seawater behaves as in contaminated systems. This is confirmed by the experiments above, but the opposite conclusion is drawn when comparing with the experiments of Rehder *et.al.* [14]. There are two important differences between the experiments presented here and those of Rehder *et.al.* [14]. Rehder *et.al.* [14] performed experiments on large bubbles in deep water and the experiments presented here are on small bubbles in shallow water. A difference between deep and shallow water is pressure. Pressure affects gas properties and dissolution, but to our knowledge pressure does not affect the part of the mass transfer mechanism governed by the mass transfer coefficient. However, the amount of surfactants do influence the mass transfer coefficient [11-13], and the level of surfactants decreases at larger depths and the water thus becomes cleaner [30]. On the other hand, larger bubbles have a higher capacity to shed small amounts of surfactants. Whether the level of contamination or bubble size is the reason for the difference between these experimentsremains uncertain. Experiments on large bubbles in shallow waters and/or small bubbles in deep water could clarify this. From the experiments presented here, we can only conclude that for small bubbles (less than 1 mm) in shallow seawater (2 meters) mass transfer is according to contaminated conditions.

5 CONCLUSIONS

Experiments with small bubbles of N_2, CO_2 and CH_4 in seawater have been conducted where bubbles were kept stationary in an observation cell. Bubble size was monitored over time and shrinkage was quantified. This shrinkage was attributed to mass transfer. Experiments were compared with a theoretical model for mass transfer. Consistency between observations and theory could only be obtained by accounting for two-way mass transfer and applying a mass transfer coefficient for contaminated conditions. Of the correlations tested, the correlation of Hughmark [9] was the most consistent with the experiments.

ACKNOWLEDGEMENTS

The study presented here was carried out within the SURE project (phase II) supported by Gassco, Total, Statoil, Wild Well Control, Safetec and SINTEF.

REFERENCES

[1] Judd A, Davies G, Wilson J, Holmes R, Baron G, Bryden I. Contributions to atmospheric methane by natural seepages on the UK continental shelf. Marine Geology. 1997;137:165-89.
[2] Olsen JE, Skjetne P. Current Understanding of Subsea Gas Release - a review. Canadian Journal of Chemical Engineering. 2016;94:209-19.
[3] Leifer I, Patro RK. The bubble mechanism for methane transport from the shallow sea bed to the surface: A review and sensitivity study. Continental Shelf Research. 2002;22:2409-28.
[4] McGinnis DF, Greinert J, Artemov Y, Beaubien SE, Wüest A. Fate of rising methane bubbles in stratified waters: How much methane reaches the atmosphere? Journal of Geophysical Research. 2006;111.
[5] Bird RB, Stewart WE, Lightfoot EN. Transport Phenomena. New York: Wiley; 1960.
[6] Clift R, Grace JR, Weber ME. Bubbles, drops, and particles. New York ; London: Academic Press; 1978.
[7] Frössling N. Über die Verdunstung falender Tropfen. Beitr Geophys. 1938;52:170-216.
[8] Higbie R. The rate of absorption of a pure gas into a still liquid during short periods of exposure. Transactions of the AIChE. 1935;31:365-89.
[9] Hughmark GA. Liquid-liquid spray column drop size, holdup, and continuous phase mass transfer. I & EC Fundamentals. 1967;58:107-14.
[10] Zheng L, Yapa PD. Modeling gas dissolution in deepwater oil/gas spills. Journal of Marine Systems. 2002;31:299-309.
[11] Takemura F, Yabe A. Rising speed and dissolution rate of a carbon dioxide bubble in slightly contaminated water. J Fluid Mech. 1999;378:319-34.
[12] Alves SS, Orvalho SP, Vasconcelos JMT. Effect of bubble contamination on rise velocity and mass transfer. Chemical Engineering Science. 2005;60:1-9.
[13] Aoki J, Hayashi K, Shigeo H, Tomiyama A. Effects of Surfactants on Mass Transfer from Single Carbon Dioxide Bubbles in Vertical Pipes. ChemEngTechnol. 2015;38:1955-64.
[14] Rehder G, Brewer PW, Peltzer ET, Friedrich G. Enhanced lifetime of methane bubble streams within the deep ocean. GeophysResLett. 2002;29.
[15] Ranz WE, Marshall WRJ. Evaporation from droplets, parts I & II. ChemEngProg. 1952;48:173-80.
[16] Sakugawa H, Handa N. Chemical studies on dissolved carbohydrates in water samples collected from the North Pacific and Bering Sea. Ocean Acta. 1985;8:185-96.
[17] Sadhal S, Johnson RE. Stokes-Flow Past Bubbles and Drops Partially Coated With Thin-Films. 1. Stagnant Cap of Surfactant Film—Exact Solution. J Fluid Mech. 1983;126:237-50.
[18] Tomiyama A, Kataoka I, Zun I, Sakaguchi T. Drag coeffcients of single bubbles under normal and micro gravity conditions. JSME International Journal, Series B. 1998;41:472-9.
[19] Maini BB, Bishnoi PR. Experimental investigation of hydrate formation behavior of a natural gas bubble in a simulated deep sea environment. Chemical Engineering Science. 1981;36:183-9.
[20] Nagamine SI. The effects of chemical dispersants on buoyant oil droplets [M.S.]. Honolulu: University of Hawaii; 2014.
[21] Masutani S, Adams E. Experimental Study of Multi-Phase Plumes with Application to Deep Ocean Oil Spills. MMS; 2000.
[22] Rzehak R. Modeling of mass-transfer in bubbly flows encompassing different mechanisms. ChemEngSci. 2016;151:139-43.
[23] García HE, Gordon LI. Oxygen solubility in seawater: Better fitting equations. Limnol Ocenaogr. 1992;37:1307-12.
[24] Hamme RC, Emerson SE. The solubility of neon, nitrogen and argon in distilled water and seawater. Deep-Sea Res. 2004;51:1517-28.

[25] Teng H, Yamasaki A. Solubility of liquid CO2 in synthetic sea water at temperatures from 278 K to 293 K and pressures from 6.44 MPa to 29.49 MPa, and densities of the corresponding aqueous solutions. Journal of chemical & engineering data. 1998;43:2-5.
[26] Wiesenburg DA, Guinasso NLJ. Equilibrium solubilities of methane, carbon monoxide, and hydrogen in water and seawater. Journal of Chemical and Engineering Data. 1979;24.
[27] Hayduk W, Laudie H. Prediction of diffusion coefficients for nonelectrolytes in dilute aqueous solutions. AiChE Journal. 1974;20:611-5.
[28] Lu W, Guo H, Chou IM, Burruss RC, Li L. Determination of diffusion coefficients of carbon dioxide in water between 268 and 473K in a high-pressure capillary optical cell with in situ Raman spectroscopic measurements. Geochimica et Cosmochimica Acta. 2013;115:183-204.
[29] Sharqawy MH, Lienhard JH, Zubair SM. The thermophysical properties of seawater: A review of existing correlations and data. Desalination and Water Treatment. 2010;16:354-80.
[30] Pakulski JD, Brenner R. Abundance and distribution of carbohydrates in the ocean. Limnology and Oceanography. 1994;39.